Characteristic features of phase diagrams describing condensation of adsorbate in narrow pores

Yu. K. Tovbin and E. V. Votyakov

State Research Center of the Russian Federation "L. Ya. Karpov Institute of Physical Chemistry," 10 ul. Vorontsovo Pole, 103064 Moscow, Russian Federation. Fax: +7 (095) 975 2450. E-mail: tovbin@cc.nifhi.ac.ru

The phase diagrams describing condensation of adsorbate in micro- and mesoporous adsorbents having slit-shaped and cylindrical pores whose size varied from 1 to 20 monolayers were constructed. The study was performed using the lattice-gas model in the quasichemical approximation to take into account the intermolecular interactions. The phase diagrams for various values of the potential arising from different types of adsorbate—adsorbent interaction were analyzed for adsorption of helium, neon, methane, and carbon tetrachloride in graphite pores. Other adsorption systems are considered and the relationship between the pressure and temperature of adsorbate condensation is discussed. A nonmonotonic variation of the critical densities for pore widths from 3 to 10 molecular diameters was found. The pattern of this variation depends on the ratio of the energy of lateral interactions of the adsorbate molecules to the energy of interaction of the adsorbate molecules with pore walls. The critical temperature decreases monotonically with a decrease in the pore width. The stronger the adsorbate interaction with the pore walls, the greater the decrease in the critical temperature.

Key words: adsorption isotherm, inert gases, methane, CCl_4, phase diagrams, micropores, mesopores, volume filling of pores, lattice-gas model, quasichemical approximation.

The conditions of phase transitions for adsorptives in micropores are known[1—8] to differ substantially from the conditions of coexistence of macroscopic phases. When an adsorptive enters pores of molecular dimensions, the interaction between the molecules makes a lower contribution to the thermodynamic functions of the system than that in the bulk phase at the same temperature. The potential of the pore walls changes the conditions of capillary condensation and thus decreases the critical temperature. The explanation of this phenomenon lies in the state of a liquid in a narrow pore that is intermediate between the three-dimensional state and a state with an intermediate dimension characterized by the parameter d ($d = 2$ for slit-shaped pores with width $H = \lambda$, where λ is the monolayer size, and $d = 1$ for cylindrical pores with diameter $D \approx \sigma$, where σ is the diameter of the molecule). It is known that, as the parameter d decreases, the critical temperature T_c tends to decrease.[9,10] As a consequence, T_c of an adsorbed fluid becomes lower than the bulk value T_c^∞ and decreases with a decrease in the pore width. The relation $|T_c - T_c^\infty|/T_c^\infty \approx A/(H + 1)^\nu$ ($\nu = 0.5$, A is a constant depending on the wall—molecule interaction potential, H is the number of monolayers in a pore) has been shown to hold for slit-shaped pores,[2] while in the case of cylindrical pores, the difference $(T_c - T_c^\infty)$ is inversely proportional to the pore radius.[3] As the width H decreases, the critical density of the adsorbate $\theta_c(H)$ for slit-shaped pores changes from 0.5 to 0.7—0.8, and the vapor pressure in the critical point decreases. In addition, the critical parameters (temperature, density, and pressure) are affected by nonuniformity of the pore walls.[7,8]

Experimental determination of the critical temperature of the adsorptive in narrow pores became possible only when adsorbents with very narrow pore size distributions appeared.[11—14] Study of the dependence of the critical temperature of nitrogen, methane, oxygen, and carbon dioxide adsorbed in mesoporous molecular sieves with an average pore radius of 1.2 to 2.1 nm [11] generally confirmed the assumptions on the dependence of the critical temperature on the radius of cylindrical pores.[3] A decrease in the critical temperature following a decrease in the capillary radius has also been observed for SF_6 adsorbed on porous glasses.[12] However, experimental investigation of the critical phenomena in micropores is faced with a number of difficulties. First, any real adsorbent has a very broad pore size distribution. Second, there are no reliable criteria indicating that the system has actually reached the critical state for adsorption under particular experimental conditions.[13,14] Third, the model adsorbents with cylindrical pores synthesized to date do not allow measurement of the critical properties of adsorbates in pores having a different geometry, in particular, in slit-shaped pores and/or in pores with a rectangular cross-section, which is typical of most car-

Published in Russian in *Izvestiya Akademii Nauk. Seriya Khimicheskaya,* No. 1, pp. 48—56, January, 2001.

1066-5285/00/5001-0050 $25.00

bon adsorbents. These difficulties can be overcome using modeling at the molecular level, which is successfully employed to determine the critical properties of adsorbed substances.

Construction of the phase diagrams of an adsorbate is even a more difficult task. This work is the first example of calculation of the phase diagrams for the adsorption of various gases, including inert gases, methane, and CCl_4, on graphite with different sizes of slit and cylindrical pores having uniform walls. In molecular modeling methods, the molecules of these adsorbates can be considered as spherical particles with a Lennard-Jones interaction potential.[15,16] The study was performed in terms of the lattice-gas model.[10] The calculation of phase diagrams using numerical methods, namely, Monte Carlo and molecular dynamics methods, provides rather accurate results (see reviews[17,18]) but is time-consuming; therefore, faster methods of calculation were used for their systematic analysis. The lattice-gas model[19–21] provides a fairly adequate description of phase diagrams not only in the vicinity of the critical point but also at lower temperatures $\tau < 0.5$ (where $\tau = T/T_c^{\infty}$), whereas the scope of numerical methods is normally limited to $\tau > 0.6$. In this work, we also considered the influence of the temperature on the pressures corresponding to the adsorbate condensation in the pores, which results in the volume filling of the pores.

Lattice model of adsorption in the pores. According to the fundamentals of the lattice model, the pore space is separated into unit volumes (units) $v_0 = \lambda^3$ (λ is the lattice constant, which is related to the parameter of the Lennard-Jones potential σ_{AA} for the adsobate molecule as $\lambda = 1.12\,\sigma_{AA}$). Then groups of units with an equal free energy of adsorption are distinguished. The energy of the adsorbate—adsorbent interaction in units of type k will be designated by Q_k ($1 \le k \le t$, where t is the number of groups of systems in the units). The intrinsic volume of the molecules is taken into account by assuming that a lattice unit cannot be occupied by more than one adsorbate molecule. Let us designate the fraction of units belonging to group k by F_k. In a slit-shaped pore, a group of units with the same properties forms a monolayer;[7,8,19,22] then $t = H$ and $F_k = 1/H$, where H is the width of the slit defined as the number of monolayers. In the core of a cylindrical pore, either one ($R_p = (h + 0.5)\lambda$) or four ($R_p = h\lambda$) units (h is an integer of λ, $h > 1$) can be located, depending on the pore radius R_p.[23] The splitting of the pore bulk into units and classification of the units into groups were performed using the data on the particle—wall interaction potential and taking into account the symmetry of the internal space of the pore. A lattice with the number of nearest neighbors $z = 6$ was used as the basic lattice model because, according to published data,[9,10,16,24] the critical parameters of this structure are in the best agreement with the experimental data for bulk fluids.

The adsorption in cylindrical pores was calculated using a "smeared" potential for the interaction of a particle located at distance y from the wall of a cylindrical pore with the radius R_p.[20,23]

$$U(y) = -2\pi\varepsilon_{As}n_s\sigma_{As}^2\left\{\sum_{j=0}^{\infty}\left(\frac{\sigma_{As}}{R_p + j\Delta - y}\right)^4 f^{(4)}\left(\frac{y}{R_p + j\Delta}\right) - \frac{2}{5}\left(\frac{\sigma_{As}}{R_p - y}\right)^{10} f^{(10)}\left(\frac{y}{R_p}\right)\right\}, \quad (1)$$

where ε_{ij} and σ_{ij} are Lennard-Jones potential parameters for the interaction of molecules of types i and j; the subscript s means surface; and the subscript A implies adsorbate. The coefficients of the polynomial function $f^{(j)}(x) = \sum_{k=0}^{9} a_{jk}x^k$ are listed in Table 1. When $R_p \to \infty$ and the distance between the molecule and the pore wall is retained, the potential given by Eq. (1) is transformed into the potential for a planar wall.[25]

A slit-shaped pore is considered to be formed by two infinite slabs of a solid parallel to the xz plane (periodical boundary conditions were imposed on the system in the directions x and z). The potential for the adsorbate interaction with the wall was calculated as the sum $U(y) + U(H - y)$, where $U(y)$ is the model potential given by Eq. (1) and $U(H - y)$ is the potential energy for the adsorbate interaction with the second pore wall. A value of the 10-4 potential was attributed to the interaction of the adsorbate molecule with each wall;[25] summation over graphite layers was performed to the tenth layer inclusively. The standard combination rules

$$\sigma_{sA} = (\sigma_{AA} + \sigma_{ss})/2,\ \varepsilon_{sA} = (\varepsilon_{AA}\varepsilon_{ss})^{1/2}, \quad (2)$$

relating the cross interactions specified by the Lennard-Jones potential parameters for individual components (Table 2) to the parameters of the surface atoms s corresponding to graphite, were used. For the basis face of graphite, the surface density of carbon atoms n_s is equal to 38.6 atoms per nm^2, and the spacing of the graphite layers Δ is 0.335 nm.

The lattice parameters $\varepsilon(r)$, $r \le R$ of the lateral interactions of adsorbate molecules were determined using the Lennard-Jones potential: $\varepsilon(r) = U_{AA}(r) =$

Table 1. Coefficients a_{jk} of the function $f^{(j)}(x)$

k	a_{4j}	a_{10j}
0	4.71239	7.73126
1	−18.84855	−77.08463
2	57.64824	563.1619
3	−134.9114	−2820.991
4	253.9246	9608.343
5	−378.7086	−21794.03
6	420.1712	32000.29
7	316.4436	−28996.07
8	141.4307	14672.09
9	−27.97551	−3162.542

Table 2. Parameters of the Lennard-Jones potential [15,16,25–27] and dimensionless parameter $\gamma = \varepsilon_{sA}/\varepsilon_{AA}$

Molecule, system	ε_{AA}/k_B/K	σ_{AA}/Å	γ
He	10.2	2.556	1.51
Ne	35.6	2.75	0.88
Ar	119.8	3.41	0.53
CH_4	148.1	3.35	0.435
CCl_4	327.0	5.881	0.29
C (carbon)	28	3.40	—
System 1	35.6	2.75	0.335
System 2	148.1	3.35	0.122
System 3	119.8	3.41	0.193
System 4	119.8	3.41	0.159
System 5	119.8	3.41	0.352

$4\varepsilon_{AA}[(\sigma_{AA}/r)^{12} - (\sigma_{AA}/r)^6]$ (the value $r/\lambda = 1$ corresponds to the minimum of this potential); R is the radius of lateral interactions measured in the numbers of coordination spheres around the central unit f. It was taken in the calculations that $R = 4$, which corresponds to the cutting radius of the interaction potential $2.5\sigma_{AA}$, normally used in numerical procedures.[17,18,21] The $\varepsilon(r)$ values are matched by the values $U_{AA}(r)$ at $r/\lambda = 1$, $\sqrt{2}$, $\sqrt{3}$, and 2, respectively.

Equations of the model. In the calculations by the lattice-gas model, we used equations[10,22,28] employed previously to study the capillary condensation in slit and cylindrical pores.[7,8,19–21,23] In each unit f the adsorbate is characterized by a particular adsorbate—adsorbent interaction energy Q_f. With allowance made for the energetic nonuniformity of the lattice units and for the interaction between the adsorbate molecules, the isotherm of multilayer adsorption has the form[10,22,28]

$$\theta(P) = \sum_{f=1}^{t} \theta_f(P) F_f, \qquad (3)$$

$$a_f P(1 - \theta_f) = \theta_f \prod_{r=1}^{R} \prod_{g \in z_f(r)} [1 + t_{fg}(r) x(r)],$$

where P is the pressure in the equilibrated bulk phase, θ_f is the coverage of a unit of layer f for slit-shaped pores or a unit of type f for cylindrical pores, and a_f is the local Henry constant for unit f; for each type of units, this constant was calculated by integration using the equation

$$a_f = \frac{1}{V_f} \int_{r \in V_f} \exp(-\beta U_{(A-C)}(r)) dr,$$

where $\beta = 1/kT$. The integration is performed over the volume of a unit with the number f ($V_f = \lambda^3$, where $\lambda = 1.12\sigma_{A-C}$). With this definition, a_f is in good agreement with the results of a strict calculation in the limit of low adsorbate densities; U_{A-C} is the potential for the adsorbate interaction with the graphite wall in unit f. The Q_f value was calculated as

$$Q_f = -\beta^{-1} \ln \left\{ \frac{1}{V_f} \int_{r \in V_f} \exp(-\beta U_{(A-C)}(r)) dr \right\}.$$

The lateral interactions (Eq. (3)) were taken into account in the quasichemical approximation, which describes the effects of direct correlation between the interacting adsorbate molecules but leaves aside the effects of indirect correlations. The index g in Eq. (3) numbers the neighboring units around the central unit f; $z_f(r)$ is the number of neighbors for a unit in layer f at distance r. The expressions for the conditional probability $t_{fg}(r)$ of the location of a particle in unit g at distance r from the "central" particle located in unit f have the following form:

$$t_{fg}(r) = \theta_{fg}^{AA}(r)/\theta_f = 2\theta_g/[\delta_{fg}(r) + b_{fg}(r)], \qquad (4)$$

$$\delta_{fg}(r) = 1 + x(r)(1 - \theta_f - \theta_g), \; x(r) = \exp[-\beta\varepsilon(r)] - 1,$$

$$b_{fg}(r) = \{[\delta_{fg}(r)]^2 + 4x(r)\theta_f\theta_g\}^{1/2};$$

where $\theta_{fg}^{AA}(r)$ is the probability that two particles occur in neighboring units f and g at distance r.

Additionally, the following normalization relations were taken into account: $\theta_{fg}^{AA}(r) + \theta_{fg}^{Av}(r) = \theta_f \equiv \theta_f^A$ и $\theta_{fg}^{vA}(r) + \theta_{fg}^{vv}(r) = \theta_f^v = 1 - \theta_f$; and $\theta_f^A + \theta_f^v = 1$ (the superscript v implies a free unit).

In a slit-shaped pore with uniform walls, the adsorption potential of the walls is symmetrical with respect to a plane in the core of the pore. This results in a symmetrical distribution of the adsorbate; therefore, the sets of equations (3) and (4) can be solved only up to the core layer rather than for the whole pore width. However, it should be borne in mind that for the core layer with the number f, the properties of units located in the neighboring layers g would be different for even and odd numbers H of monomolecular layers in the pore.[7,8,19–21] In the case of cylindrical pores, the number of equations in set (3) decreases due to the circular symmetry of the arrangement of units of different types with respect to the core of the cylinder cross-section.[23]

The equilibrium distribution of particles over units of different types was found from the set of equations (3) by the Newtonian iteration method. The accuracy of the solution of this set is at least 0.1%.

Objects of investigation. Let us consider carbon adsorbents with slit-shaped pores adsorbing helium, neon, methane, and carbon tetrachloride. This makes it possible to find out how the change in the depth of the potential well of different adsorbents influences the patterns of phase diagrams. The dimensionless coefficient $\gamma = \varepsilon_{sA}/\varepsilon_{AA}$ (see Table 2), which characterizes the energy difference between the interaction of the adsorbate with the wall and the interaction between adsorbate molecules, was chosen as the main parameter for the comparison of various systems. The higher this coefficient,

the greater the influence of the potential of the wall on the adsorbate condensation in the pores. The decrease in the γ value points to the crucial role of intermolecular interactions because the effect of the pore walls manifests itself only in the fact that the volume accessible for molecules decreases upon condensation. In the series of adsorbates studied, the γ value varies from 1.51 (He) to 0.29 (CCl_4).

Now we will take slit-shaped pores as an example to discuss the variation of the pattern of phase diagrams *vs.* the parameter γ ranging from 0.1 to 0.3, which corresponds to pores whose walls weakly attract the adsorbate molecules. Characteristic features of phase diagrams for microporous systems are also of interest. Comparison of the results obtained for slit-shaped pores with the data for cylindrical pores showed how the geometric parameters affect the phase diagrams.

All the results of calculations of phase diagrams are shown in the corrected coordinates τ—ρ ($\rho = \theta(\sigma/\lambda)^3$ is the numerical density of the fluid for the system volume expressed in the units of volume of the particles as solid spheres). The ρ units are normally used in numerical methods of investigations.[18] For a rigid (noncompressible) lattice, $\rho = \theta/1.41$ because $\lambda = \sigma(2)^{1/6}$. The use of corrected coordinates is associated with the quasichemical approximation of calculations. It is known[9,10] that the use of the quasichemical approximation in the critical region provides only qualitative results. Thus, with allowance for the nearest neighbors ($R = 1$), we obtain the expression $T_c^\infty \approx 1.2\varepsilon_{AA}/k_B$ (k_B is the Boltzmann constant); in the case of $R = 4$, the expression is transformed into $T_c^\infty \approx 2.26\varepsilon_{AA}/k_B$. The use of relative τ values in the corrected coordinates T/T_c^∞—ρ permits some leveling of the difference between the results of approximate calculations of T_c^∞, including those in the quasi-chemical approximation.[16,29,30] In particular, in these corrected coordinates, the difference between the critical temperatures calculated in terms of the lattice model and those found using exact numerical methods is ~6%.

The limiting ρ value in these calculations is ~0.71. If a more perfect model with a "soft" lattice,[31] in which the lattice constant varies with concentration, thus ensuring the minimum of free energy, is employed instead of the model with a rigid lattice, the limiting value is equal to ~0.80. This is in good quantitative agreement with the results of calculations for porous systems performed by the numerical Monte Carlo and molecular dynamics methods for the liquid-phase branch of phase diagrams.[19—21] In the first approximation, all calculations based on the rigid-lattice model can be converted to the "soft"-lattice model by merely multiplying the density ρ by a factor of ~1.125.[31] Due to the foregoing, the calculation of phase diagrams can be substantially facilitated and the influence of the pore width and potential functions of the adsorbate—adsorbent system on the pattern of the curves of adsorbate condensation can be studied. The gas-phase branch of the phase diagram in the lattice-gas model is shifted somewhat to higher densities with respect to that found by Monte Carlo or molecular dynamics calculations[19—21]; however, these differences are insignificant for the present study.

Slit-shaped pores. *Graphite systems.* For helium, neon, methane, and carbon tetrachloride, calculations of phase diagrams were performed for the pore width H ranging from 1 to 20 monolayers. The phase diagrams of all the adsorption systems are qualitatively similar. The vapor—liquid equilibria of molecules of this type in bulk phases have long been described using the principle of corresponding states.[16,29,30] The constructed phase diagrams show that the same principle can also be employed to describe the thermodynamic properties of an adsorbate in narrow pores. This is exemplified in Fig. 1, which represents the calculated phase diagrams of methane in slit-shaped pores of different widths in graphite (the numbers in all figures mean the pore width). The change in the pore size brings about similar effects for all the systems studied.

Under the action of the adsorption potential of the walls, the curve of condensation of adsorbate shifts downwards with respect to the vapor—liquid curve for the bulk system on an open surface (*i.e.*, outside the pore). The strong field of the adsorbent markedly increases the density of the gas branch. As a consequence, the densities of both coexisting phases, especially the vapor phase, are higher in the pores than in the bulk.

For small pore sizes $H = 1$ and 2, condensation curves have a symmetrical shape, similar to that of the curves for the bulk phase. This is due to the fact that all the units in the lattice are equivalent and at different H they differ only by the number of nearest neighbors z ($z = 4$ for $H = 1$; $z = 5$ for $H = 2$, and $z = 6$ for the bulk phase for which $H = \infty$). In the range of sizes H from 3 to 20, all the condensation curves are shifted to higher densities. As the pore size increases, the critical tem-

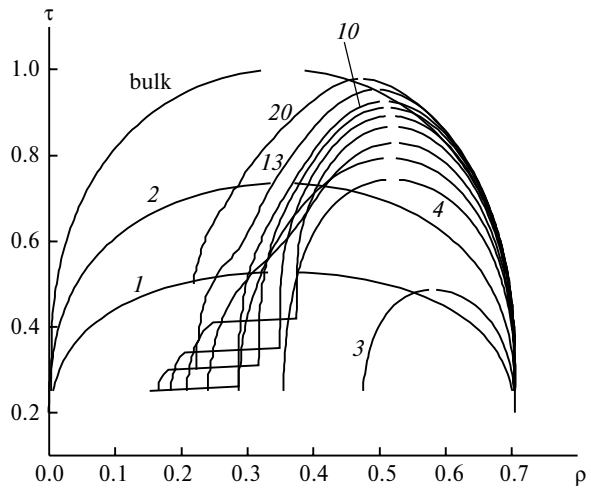

Fig. 1. Phase diagram of methane in slit-shaped pores of graphite of different widths. The numbers of the curves correspond to the pore width.

perature increases monotonically, while the critical density depends on the pore size in a more complex manner. As the pore width H increases from 3 to 8, the phase diagrams display first a minimum (a decrease in the critical density) and then a maximum (an increase in the critical density); subsequently, the critical density tends monotonically to the value typical of the bulk phase. This "zigzag" is observed for each of the four systems studied.

It should be noted that the range of ε_{AA} values considered covers the sizes of the molecules of inert gases (Ar, Kr, Xe), nitrogen, hydrogen, oxygen, carbon oxide and monoxide, and many others. This means that the nonmonotonic variation of the critical density with the pore width varying from micro- to mesopores is universal. Meanwhile, as the coefficient γ decreases, the region of existence of the two-phase system becomes somewhat broader, which is slightly visible for $H = 3$ and is more pronounced for greater H. When $\tau < 0.5$, the phase diagrams exhibit steps caused by layer-by-layer adsorption on the pore walls. The absence of these steps in the case where $0.25 < \tau < 0.5$ means that they are formed at lower temperatures,[7,8,21,23] which are not considered in this study.

Model systems. We considered four model systems in which the interaction of an adsorbed molecule with a neighboring molecule is stronger than with the wall. In system 1, the adsorbate (neon) atoms are characterized by an ε_{sA} value about 3 times smaller than that in the real neon—graphite system, while the potential ε_{AA} for the interaction between neon atoms is retained. System 2 consists of methane molecules the potential of interaction of which with the walls is reduced approximately 3.6-fold. In systems 3 and 4 (based on the argon—graphite system), the depth of the potential well for the interaction of argon atoms with one another ε_{AA}/k_B has increased from 118.9 K to 750 and 1100 K, respectively (the enhancement of the interaction with the wall is found from Eq. (2)). The phase diagram of model system 2 is presented in Fig. 2. The patterns of the phase diagrams of other model systems are similar.

The curves for pore widths from 3 to 8 shown in Fig. 2 differ markedly from the curves presented in Fig. 1: the critical temperature increases monotonically starting from $H = 1$; the critical density has one maximum at $H = 8$—10. The displacement of all curves to higher densities is less pronounced, and two-phase regions are substantially larger.

The γ values for the model systems cover the energy characteristics of many real objects. The range of these objects includes inert gases and methane in weakly adsorbing porous solids (including polymeric matrices) and adsorptives such as Hg ($\varepsilon_{AA}/k_B = 851$ K) and $SnCl_4$ ($\varepsilon_{AA}/k_B = 1550$ K),[16] which are adsorbed in the vast majority of cases without specific interactions. (The calculated phase diagrams can be used to interpret the phase state of mercury in the narrow pores of almost any adsorbent.) Note that mercury porosimetry is widely

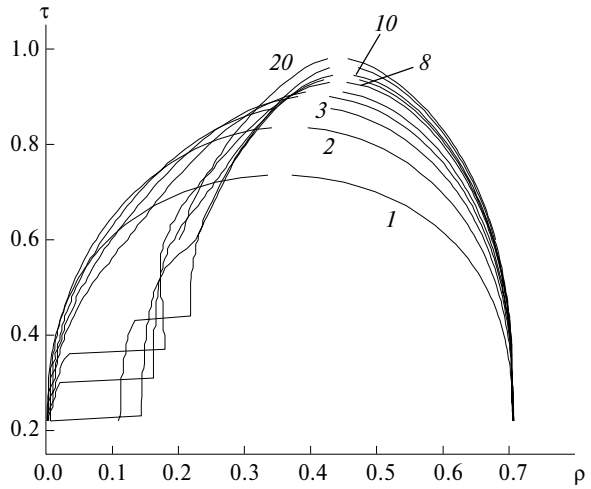

Fig. 2. Phase diagram of a methane-contaning model system 2 for slit-shaped pores. For designations, see Fig. 1.

used to determine pore sizes in the mesoporous range.[32,33] Systems containing adsorbate molecules like CH_3OH ($\varepsilon_{AA}/k_B = 507$ K) and CH_3Cl ($\varepsilon_{AA}/k_B = 855$ K) in numerous adsorbents including graphite should be mentioned as systems with intermediate γ values.

The coefficient γ. For model systems, the coefficient $\gamma = \varepsilon_{sA}/\varepsilon_{AA}$ was introduced, which varies from 0.335 to 0.122 (see Table 2). The upper region of its magnitudes corresponds to "strong" adsorption ($\gamma > 0.29$). This fact is explained in the following way. The γ parameter was found from the Lennard-Jones potentials, although in a more rigorous approach, it should have been determined using the total energy of the molecule in the bulk phase and near the pore wall taking into account the contributions of the second and more remote neighbors. In view of the fact that the radius of the neon atom is about twice as small as the radius of the CCl_4 molecule, the particular calculation of the total energy of lateral interactions between the molecules and the energy of their interactions with the pore walls accounts for the overlap of the γ values corresponding to the cases of so-called "weak" and "strong" adsorption. Therefore, the range of γ should apparently be split into two sections, namely, $\gamma < 0.2$ (weak adsorption; the typical phase diagrams are shown in Fig. 2) and $\gamma > 0.4$ (strong adsorption, the typical phase diagrams are shown in Fig. 1). In the intermediate region, $0.2 < \gamma < 0.4$, the shape of the phase diagram cannot be predicted reliably from the parameters of potential curves, and particular numerical analysis of the total energies of interaction of the adsorbate molecules with the walls and with one another is required.

The fundamental difference of the classification of adsorption systems in terms of the coefficient γ proposed here is illustrated by phase diagrams of microporous systems with $H = 1$—3 (Fig. 3). As noted above, the curves with $H = 1$ and $H = 2$ are symmetrical and are similar to the condensation curve for the bulk phase;

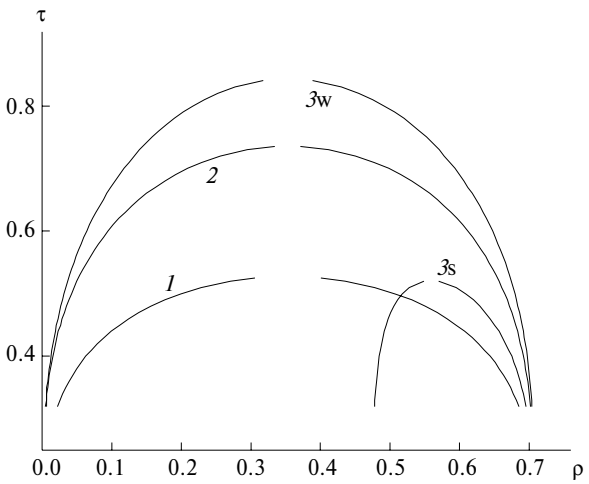

Fig. 3. Phase diagrams of systems with micropores (letters w and s refer to the cases of weak and strong adsorption, respectively).

however, the condensation effect is observed at a lower critical temperature due to the smaller number of neighboring molecules. For a pore with size $H = 3$, the shapes of the segregation curves for weak and strong adsorption are different. In the former case, the critical temperature increases monotonically as the pore size varies from 2 to 3, while the critical density shifts somewhat to greater values. In the case of strong adsorption, both the critical temperature and the critical density change sharply as H changes from 2 to 3. As this takes place, the critical temperatures for pores with $H = 3$ and $H = 1$ approach each other. This indicates that, as the pore is being filled by the adsorbate, initially, the first two layers are covered successively and the overall density ρ shifts to greater values and then the adsorbate is condensed in the last layer. The conditions of adsorbate condensation are evidently the same in the first layer of a pore with width $H = 1$ and in the last layer of a pore with $H = 3$. In other words, the pre-adsorbed molecules decrease the effective pore width at $H = 3$. A similar situation is observed for filling of a pore with $H = 4$ in the cases of weak and strong adsorption.

A layer-by-layer covering of the pore walls in the case of strong adsorption does not mean that the state of the near-wall layer of molecules in the pore volume remains invariable during their condensation. This does not mean that condensation in the pore bulk proceeds irrespective of the state of pre-adsorbed molecules or that the near-surface layer does not participate in the condensation process and is not affected by the phase state of the rest of the pore. Figure 4 shows the change in the coverage of the near-surface and intermediate layers and the overall pore coverage at $H = 3$ for strong (*a*) and weak (*b*) adsorption. In the case of weak adsorption (*b*), all curves follow similar patterns: as the temperature increases, the loop disappears. Integration of the loop according to the Maxwell rule[9,10,16,29,30] is known to determine the position of the cutting line

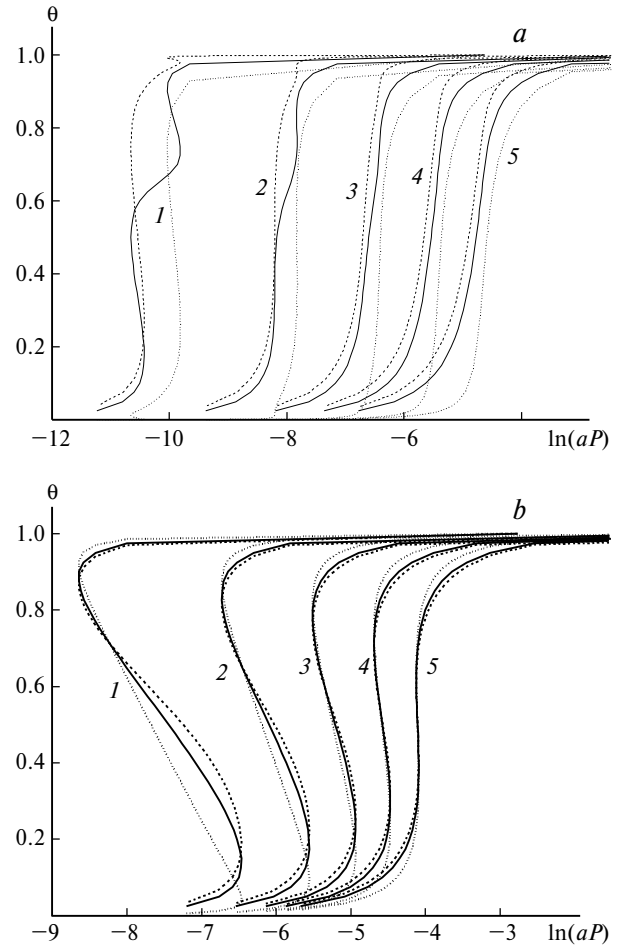

Fig. 4. Isotherms for coverage of the near-surface (dashed lines) and intermediate (dotted lines) layers in a slit-shaped pore with $H = 3$ for strong (*a*) and weak (*b*) adsorption at various reduced temperatures $\tau = 0.4$ (*1*), 0.5 (*2*), 0.6 (*3*), 0.7 (*4*), and 0.8 (*5*); continuous lines are full adsorption isotherms.

segment for the density step upon phase transition and the condensation pressure of the adsorbate. In the case of strong adsorption, the difference between these curves is more pronounced. At the lowest temperature (curve *1*), not only the density in the second intermediate layer changes upon the phase transition but also an additional loop (*i.e.*, its own density step) occurs in the surface layer at condensation pressures in the intermediate layer. This means that all the adsorbate molecules in the system are involved collectively in the segregation phase transition. Otherwise, if the surface layer had not participated in the phase transition of molecules of the intermediate layer, its density would have remained constant after it reached a particular value.

Cylindrical pores. The effects described above should substantially depend on the geometry of the pore cross-section because it determines the ratio of the numbers of near-surface and internal pore units.[23] Let us consider cylindrical pores differing in diameters. The minimum diameter H is four, due to the specific character of the

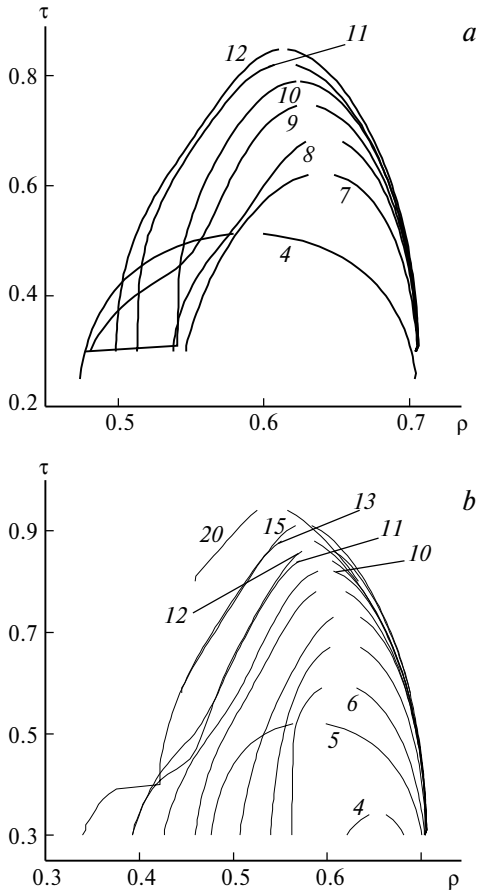

Fig. 5. Phase diagrams for condensation of helium (*a*) and methane (*b*) in cylindrical pores of graphite. For designations, see Fig. 1.

lattice model for a cylindrical pore containing breaks instead of a perfect circle.[23] The phase diagrams for condensation of helium and methane in graphite (Fig. 5), as in the case of slit-shaped pores, exhibit a zigzag as the pore diameter increases, and steps at low temperatures; in addition, the critical density of the fluid approaches the density of the liquid phase. Thus, the nonmonotonic variation of the critical densities found for strong adsorption in slit-shaped pores is also retained for cylindrical pores.

The case of weak adsorption in model systems 3—5 is shown in Fig. 6. System 5 corresponds to a real Ar—graphite system with cylindrical pores; its σ_{AA} parameter is equal to that of argon but $\varepsilon_{AA}/k_B = 250$ K. As in the case of slit-shaped pores, the critical density follows an extremal type of dependence on the pore width as the diameter changes from 8 to 10 lattice constants. For the pore diameter $D = 9$, the highest critical density was observed. Note that for systems 3 and 4 (Ar—graphite), the gas-phase branches for pores with $D = 8$ and 10 are arranged much closer to each other than to the gas-phase branch for pores with a diameter of 9 (the γ coefficient lies in the intermediate region, which requires special numerical analysis).

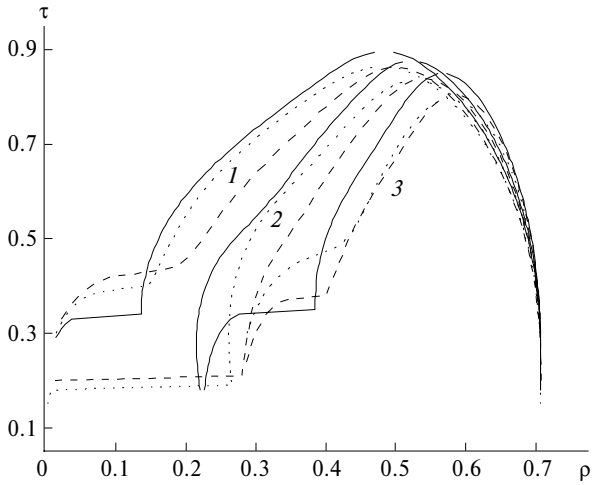

Fig. 6. Phase diagrams for weak adsorption for model systems 3 (*1*), 4 (*2*), and 5 (*3*) in cylindrical pores with diameters of 8 (dotted lines), 9 (dashed lines), and 10 (continuous lines).

Temperature dependences of pressures corresponding to the adsorbate in pores. In the general case, attraction of the adsorbate by both pore walls increases the coverage of a micropore compared with that observed for an open surface at the same temperature. To analyze the properties of an adsorbate in narrow pores, in addition to the condensation curves, one needs to know the temperature dependences of the saturated vapor pressure at which filling of the micropore volume occurs. The attraction of molecules by pore walls markedly decreases this pressure. Figure 7 shows schematically the variation of the position of the saturated vapor pressure curve on the $P—T$ cross-section of the phase diagram for the bulk phase and a slit-shaped pore with width H (in the case of cylindrical pores, a similar diagram is observed; here, H is the pore diameter). The line AB corresponds to the

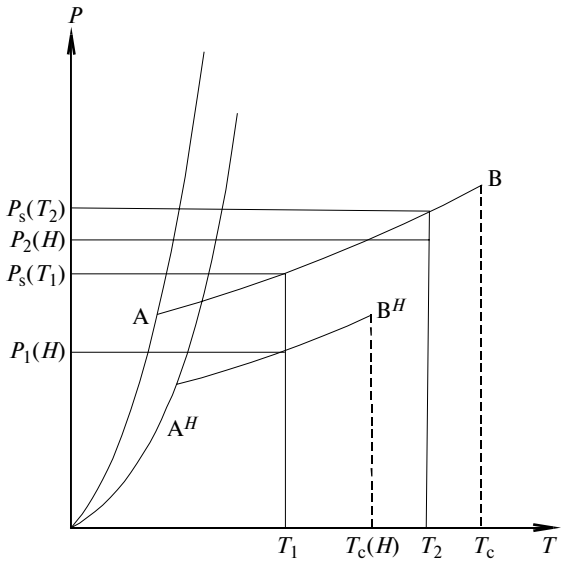

Fig. 7. Scheme of the $P—T$ cross-section of the phase diagram for adsorption in the pores and for the bulk liquid.

bulk phase (A is the triple point, B is the critical point) and line $A^H B^H$ corresponds to a pore with size H. Calculations showed that the differences become more pronounced as H decreases. In narrow pores, two variants of adsorption are realized, depending on the temperature of the experiment: $T_1 < T_c(H)$ and $T_2 > T_c(H)$, where $T_c(H)$ is the critical temperature of the adsorbate in a pore with the width H. When the temperature is T_1 and the pressure has increased to $P_1(H)$, the line $A^H B^H$ is intersected and the condensation of the adsorbate takes place in the pore. In a closed system of pores, phase transition during condensation takes place; however, a real experiment is carried out in an open system; therefore, complete filling of a pore with liquid adsorbate was observed. The $P_1(H)$ value is an analog of the saturated vapor pressure of the bulk phase. At temperature T_2, which exceeds the critical temperature, the filling of pore volume occurs without phase transition. In both cases, filling of micropores stops at some pressure $P_{1,2}(H)$ lower than P_s, which is the saturated vapor pressure above the bulk liquid at the same temperature.

Calculations showed that the values $P_1(H)$ and P_s are substantially different. This difference reaches the maximum for a pore with the width $H = 1$. As the temperature decreases, the range of the decrease of the $P_1(H)$ values corresponding to the phase transformations of helium, neon, methane, and carbon tetrachloride reaches the following values (the given values are the natural logarithms of the pressures corresponding to the greatest deviations from P_s): up to −75 (He), −52 (Ne), −36 (CH_4), and −42.5 (CCl_4). It can be stated that the volume filling of a pore of a monomolecular width takes place at very low pressures.

It is evident that the size of the region of the maximum decrease in the critical pressure for $H = 1$ is determined by the properties of the system and by the temperature. For systems with cylindrical pores shown in Fig. 5, the calculated pressure changes are approximately twice as small.

The obtained temperature dependences of the condensation pressure can be represented more clearly by dividing them by the condensation pressure in the bulk gas phase P_s. From Eqs. (3) and (4), the relation $\ln(P_s)/(\beta\varepsilon_{AA}) = -4.79$ can be easily derived. This is the limiting value for each family of the temperature dependences $\eta = \ln(P_1(H))/(\beta\varepsilon_{AA})$ for different gases following an increase in the pore size of the adsorbent. Typical temperature dependences of η for all the systems studied presented in relation to carbon tetrachloride in graphite pores indicates that the pores are rapidly filled as the temperature decreases (Fig. 8). The curves have discontinuities on the left side; to continue them, it is necessary to know the position of the curve of the liquid—solid phase transition. For this purpose, one should calculate the melting point of the substance in the corresponding pores (this problem has not been solved by now; for none of the systems, the precise position of the triple points A^H is known). The points

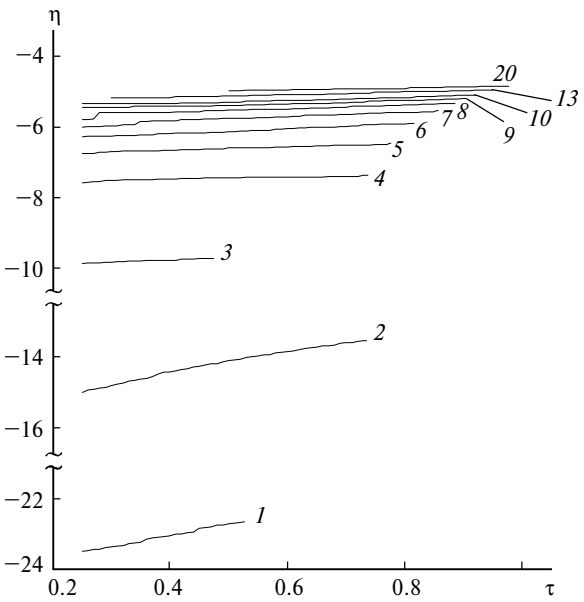

Fig. 8. Temperature dependences of the condensation pressures of carbon tetrachloride η in slit-shaped pores of different widths. For designations, see Fig. 1.

where the η(τ) curves end on the right side are determined by the critical temperatures of the corresponding phase diagrams. The accuracy of their determination (due to the calculation algorithm) amounts to 0.2%. The figure demonstrates the degree to which the potential of the walls influences the pressures of adsorbate condensation for different pore widths H.

The calculated η(τ) dependences can be considered linear; therefore, they are defined adequately by the coordinates (τ and η(τ)) of the end points for low (τ_1) and high (τ_2) temperatures. Table 3 shows the η(τ) dependences for helium, neon, methane, and carbon tetrachloride in slit-shaped pores and for helium and methane in cylindrical pores of graphite, as well as the η(τ) curves for model system 2 in slit-shaped pores of different widths. A small deviation of the η(τ) dependence from linearity is observed only for $H = 2$ for methane and carbon tetrachloride and for model system 2.

The resulting η(τ) dependences reflect the characteristic features of interaction of the adsorbate molecules with the pore walls. These data can be used to determine the conditions of filling of pore volume for different systems and, especially, to verify the applicability of the empirical Dubinin—Radushkevich equation and its generalizations.[32,33]

In conclusion, we will summarize some results of this study. The critical properties of spherical molecules with the Lennard-Jones interaction potential in carbon slit-shaped pores of different widths were studied. The phase diagrams for pore sizes ranging from 1 to 20 molecular diameters were calculated based on the lattice-gas model. A monotonic decrease in the critical temperature following a decrease in the pore width was noted; the stronger

Table 3. Initial and final values of the $\eta(\tau)$ function calculated for the adsorption systems studied*

H	Slit-shaped pores											
	Ne				CCl_4				Model system 2			
	τ_1	$\eta(\tau_1)$	τ_2	$\eta(\tau_2)$	τ_1	$\eta(\tau_1)$	τ_2	$\eta(\tau_2)$	τ_1	$\eta(\tau_1)$	τ_2	$\eta(\tau_2)$
1	0.25	28.04	0.527	27.21	0.25	23.49	0.527	22.64	0.25	10.70	0.527	10.02
2	0.25	17.37	0.735	15.74	0.25	14.97	0.735	13.51	0.25	7.675	0.735	6.933
3	0.25	10.37	0.47	10.15	0.25	9.86	0.475	9.70	0.25	6.85	0.833	6.162
4	0.25	7.83	0.736	7.58	0.25	7.55	0.738	7.36	0.25	6.33	0.871	5.705
5	0.25	6.92	0.763	6.60	0.25	6.73	0.778	6.45	0.25	6.03	0.889	5.45
6	0.25	6.41	0.806	5.95	0.25	6.26	0.816	5.88	0.25	5.82	0.90	5.28
7	0.25	6.09	0.852	5.57	0.25	5.97	0.858	5.53	0.25	5.48	0.91	5.15
8	0.25	5.58	0.881	5.34	0.25	5.78	0.885	5.32	0.25	5.36	0.92	5.07
9	0.25	5.43	0.90	5.20	0.25	5.42	0.906	5.18	0.25	5.28	0.93	5.00
10	0.25	5.32	0.92	5.10	0.25	5.32	0.921	5.08	0.25	5.22	0.94	4.94
13	0.30	5.15	0.949	4.94	0.30	5.14	0.951	4.93	0.25	5.10	0.96	4.88
20	0.50	4.95	0.98	4.83	0.50	4.95	0.978	4.83	0.80	4.86	0.98	4.82

H	Slit-shaped pores								D	Cylindrical pores							
	He				CH_4					He				CH_4			
	τ_1	$\eta(\tau_1)$	τ_2	$\eta(\tau_2)$	τ_1	$\eta(\tau_1)$	τ_2	$\eta(\tau_2)$		τ_1	$\eta(\tau_1)$	τ_2	$\eta(\tau_2)$	τ_1	$\eta(\tau_1)$	τ_2	$\eta(\tau_2)$
1	0.25	41.40	0.527	40.50	0.25	19.78	0.527	18.95	4	0.32	26.58	0.39	26.31	0.30	11.24	0.52	10.61
2	0.25	24.87	0.735	23.03	0.25	12.75	0.735	11.45	5	0.25	18.78	0.513	17.40	0.30	9.12	0.34	9.03
3	0.25	12.37	0.47	11.90	0.25	9.24	0.486	9.08	6	0.29	8.44	0.515	8.39	0.30	7.59	0.59	7.20
4	0.25	9.02	0.735	8.49	0.25	7.17	0.743	7.00	7	0.30	7.50	0.62	7.27	0.30	6.81	0.67	6.51
5	0.25	7.79	0.688	7.25	0.25	6.45	0.794	6.21	8	0.30	6.93	0.68	6.57	0.30	6.38	0.73	6.03
6	0.25	6.52	0.777	6.27	0.25	6.04	0.83	5.73	9	0.30	6.51	0.745	6.08	0.30	6.10	0.78	5.69
7	0.25	5.98	0.835	5.77	0.25	5.80	0.866	5.44	10	0.30	6.24	0.789	5.76	0.30	5.89	0.82	5.47
8	0.30	5.70	0.686	5.48	0.25	5.63	0.892	5.25	11	0.30	5.99	0.82	5.54	0.30	5.74	0.84	5.32
9	0.30	5.52	0.893	5.29	0.25	5.51	0.91	5.13	12	0.30	5.81	0.848	5.38	0.30	5.62	0.86	5.22
10	0.30	5.40	0.91	5.16	0.25	5.42	0.926	5.05	13	—	—	—	—	0.30	5.53	0.88	5.13
13	0.30	5.20	0.945	4.97	0.30	5.12	0.953	4.92	15	—	—	—	—	0.58	5.24	0.91	5.02
20	0.80	4.89	0.975	4.84	0.50	4.95	0.979	4.83	20	—	—	—	—	0.80	4.97	0.94	4.89

* The minus sign at all η values is omitted.

the interaction of the adsorbate with the pore walls, the more pronounced this effect. A new effect of nonmonotonic variation of the critical density of the adsorbate *vs.* pore width during capillary condensation was found. The type of pore cross-section (a slit or cylinder) does not influence this effect. However, its character depends on the ratio of the energies of interaction of an adsorbate molecule with the wall and with a neighboring adsorbate molecule. The introduction of the coefficient γ characterizing this ratio makes it possible to distinguish two cases corresponding to weak and strong adsorption. In the case of strong adsorption, the critical density varies according to a zigzag pattern for H ranging from 3 to 10. For weak adsorption, the critical density has a maximum in the range of $H = 8—10$.

The above-indicated fact is of fundamental importance for interpretation of the experimental adsorption isotherms on micro- and mesoporous sorbents and for interpretation of data on the self-diffusion and mass transfer coefficients. In real adsorbents with a very broad pore size distribution, the type of phase state of the adsorbate depends substantially on the pore size in the considered region of the adsorbent and on the pore sizes in the adjacent regions. Therefore, the calculation of the phase distribution of the adsorbate requires information not only on the pore size distribution function but also on the adsorbent structure. The discovered nonmonotonic dependence of the critical density on the pore width makes these calculations more complex, which hampers interpretation of experimental data on the equilibrium and transport characteristics of adsorption at the molecular level.

References

1. M. E. Fisher and H. Nakanishi, *J. Chem. Phys.*, 1981, **75**, 5857.
2. H. Nakanishi and M. E. Fisher, *J. Chem. Phys.*, 1983, **78**, 3279.
3. R. Evans and U. M. B. Marconi, *J. Chem. Phys.*, 1986, **84**, 2376.
4. P. Tarasona, U. M. B. Marconi, and R. Evans, *Mol. Phys.*, 1987, **60**, 573.
5. E. Bruno, U. M. B. Marconi, and R. Evans, *Physica A*, 1987, **141**, 187.

6. A. de Kreizer, T. Michalski, and G. H. Findenegg, *Pure Appl. Chem.*, 1991, **63**, 1495.
7. Yu. K. Tovbin and E. V. Votyakov, *Langmuir*, 1993, **9**, 2652.
8. E. V. Votyakov and Yu. K. Tovbin, *Zh. Fiz. Khim.*, 1994, **68**, 287 [*Russ. J. Phys. Chem.*, 1994, **68** (Engl. Transl.)].
9. T. L. Hill, *Statistical Mechanics. Principles and Selected Applications*, McGraw-Hill Book Comp. Inc., New York, 1956.
10. Yu. K. Tovbin, *Teoriya fiziko-khimicheskikh protsessov na granitse gaz—tverdoe telo* [*The Theory of Physicochemical Processes at the Gas—Solid Interface*], Nauka, Moscow, 1990, 288 pp. (in Russian).
11. K. Morishige, M. Fujii, M. Uga, and D. Kinukama, *Langmuir*, 1997, **13**, 3494.
12. M. Thommes and G. H. Findenegg, *Langmuir*, 1994, **10**, 4270.
13. J. Rathousky, A. Zukal, O. Franke, and G. Schulz-Ekloff, *Farady Trans.*, 1995, **91**, 937.
14. P. Ravikovich, S. C. Domhnail, A. V. Neimark, F. Schutz, and K. K. Unger, *Langmuir*, 1995, **11**, 4765.
15. N. N. Avgul', A. V. Kiselev, and D. P. Poshkus, *Adsorbtsiya gazov i parov na odnorodnykh poverkhnostyakh* [*Adsorption of Gases and Vapors on Homogeneous Surfaces*], Khimiya, Moscow, 1975, 384 pp. (in Russian).
16. J. O. Hirschfelder, C. F. Curtiss, and R. B. Bird, *Molecular Theory of Gases and Liquids*, Wiley, New York, 1954.
17. D. Nicholson and N. D. Parsonage, *Computer Simulation and the Statistical Mechanics of Adsorption*, Academic Press, London, 1982.
18. Yu. K. Tovbin, *Metod molekulyarnoi dinamiki v fizicheskoi khimii* [*Method of Molecular Dynamics in Physical Chemistry*], Nauka, Moscow, 1996, 128 pp. (in Russian).
19. Yu. K. Tovbin and T. V. Petrova, *Zh. Fiz. Khim.*, 1995, **69**, 127 [*Russ. J. Phys. Chem.*, 1995, **69** (Engl. Transl.)].
20. E. V. Votyakov, Yu. K. Tovbin, J. M. D. Macelroy, and A. Roche, *Langmuir*, 1999, **15**, 5713.
21. A. M. Vishnyakov, E. M. Piotrovskaya, E. N. Brodskaya, E. V. Votyakov, and Yu. K. Tovbin, *Zh. Fiz. Khim.*, 2000, **74**, 221 [*Russ. J. Phys. Chem.*, 2000, **74** (Engl. Transl.)].
22. Yu. K. Tovbin, *Proc. Intern. Conf. "Electrodynamics of Interface. Quantum Effects in Adsorption Films"*, *Telavi*, *1984*, Metsnieroba, Tbilisi, 1986, p. 210.
23. Yu. K. Tovbin and E. V. Votyakov, *Zh. Fiz. Khim.*, 1998, **72**, 1885 [*Russ. J. Phys. Chem.*, 1998, **72** (Engl. Transl.)].
24. O. Yu. Batalin, Yu. K. Tovbin, and V. K. Fedyanin, *Zh. Fiz. Khim.*, 1980, **53**, 3020 [*Russ. J. Phys. Chem.*, 1980, **53** (Engl. Transl.)].
25. W. A. Steele, *The Interactions of Gases with Solid Surfaces*, Pergamon, New York, 1974.
26. W. L. Jorgensen, C. J. Madura, and C. J. Swenson, *J. Am. Chem. Soc.*, 1984, **106**, 6638.
27. S. Sokolowski and J. Fischer, *Mol. Phys.*, 1990, **71**, 393.
28. Yu. K. Tovbin, *Dokl. Akad. Nauk SSSR*, 1990, **312**, 918 [*Dokl. Chem.*, 1990 (Engl. Transl.)].
29. I. R. Prigozhin, *Molekulyarnye teorii rastvorov* [*Molecular Theories of Solutions*], Khimiya, Moscow, 1987, 450 pp (in Russian).
30. N. A. Smirnova, *Molekulyarnaya teoriya rastvorov* [*Molecular Theory of Solutions*], Khimiya, Leningrad, 1987, 360 pp.(in Russian).
31. Yu. K. Tovbin, M. M. Senyavin, and L. K. Zhidkova, *Zh. Fiz. Khim.*, 1999, **73**, 304 [*Russ. J. Phys. Chem.*, 1999, **73** (Engl. Transl.)].
32. S. J. Gregg and K. G. W. Sing, *Adsorption, Surface Area and Porosity*, Academic Press, London, 1982.
33. T. G. Plachenov and S. D. Kolosentsev, *Porometriya* [*Porometry*], Khimiya, Leningrad, 1988, 175 pp. (in Russian).

Received December 29, 1999;
in revised form May 17, 2000